Journal of Catalysis **209,** 318–330 (2002)
doi:10.1006/jcat.2002.3651

Preparation of Nickel–Tungsten Bimetallic Carbide Catalysts

Tiancun Xiao, Haitao Wang, Andrew P. E. York,[1] V. Cliff Williams,[2] and Malcolm L. H. Green[3]

Wolfson Catalysis Centre, Inorganic Chemistry Laboratory, University of Oxford, South Parks Road, Oxford OX1 3QR, United Kingdom

Received August 13, 2001; revised February 4, 2002; accepted April 16, 2002

A series of nickel and tungsten bimetallic oxides have been prepared using the solid state reaction of nickel nitrate and tungsten trioxide, which were carburised under temperature-programmed conditions with a mixture of 20% CH_4/H_2 and 10% C_2H_6/H_2 to prepare the corresponding carbides. A GC–MS was employed to monitor the carburisation process, and the resulting oxides and carbides have been characterised with X-ray diffraction (XRD), laser Raman spectroscopy, scanning electron microscopy (SEM), and transmission electron microscopy (TEM). It is shown that a greater proportion of nickel tungstate is formed at a high nickel-to-tungsten ratio during the solid state reaction. At a Ni/(Ni + W) (molar) ratio of 0.4, the surface is completely covered with $NiWO_4$, although the bulk phase is completely converted to $NiWO_4$ when the Ni/W ratio approaches unity. Carburising the oxide with a mixture of 20% CH_4/H_2 or 10% C_2H_6/H_2 leads to β-W_2C. However, the carbide is formed at a lower carburisation temperature when using 10% C_2H_6/H_2 instead of 20% CH_4/H_2. The nickel metal is either highly dispersed in or occupies the tungsten carbide lattice. After passivation, the surface of the Ni and W carbide is converted into the oxide of $NiWO_4$, although the bulk structure is still that of β-W_2C carbide. The carbon content in the bimetallic carbide decreases and the carbide particle size becomes larger with increasing nickel content.

INTRODUCTION

Transition metal carbides possess significantly modified physical and chemical properties compared to the parent metals due to the incorporation of carbon into the metal lattice (1, 2). There have been several methods for preparation of transition metal carbides (3–9), among which the TPR method, pioneered by Boudart and co-workers (4, 5), has been widely used to prepare high-surface-area carbides. In the TPR method, metal oxides are treated with gas mixtures of light hydrocarbons diluted with hydrogen. The properties of carbides prepared by the TPR method are very dependent on the synthesis conditions employed (3, 10–16).

Most of the studies on transition metal carbides reported so far have focussed on binary compounds, e.g., monometallic carbides, because of the complexity of the multimetallic systems. Only a few studies have focussed on the preparation and application of bimetallic carbides (17–19). Carbide phases can exist over a broad composition range and with appreciable concentrations of dopants, but their physical properties are quite sensitive to the composition. It is possible to induce positive interactions between metal and nonmetal elements by introducing other elements into the binary carbide phase. Such synergies have been successfully demonstrated by simultaneous substitution of metal and nonmetal elements into the binary carbide Mo_2C (19, 20).

Nickel and tungsten bimetallic sulfide material has been identified as one of the most effective catalysts for HDN, the Ni content having a very strong effect on the catalytic performance. However, no study on the preparation of NiW bimetallic carbides and the effects of the Ni content on structure has yet been reported. In this investigation, a series of bimetallic NiW carbide materials have been synthesised by the TPRe method. The effect of different carburising agents and of Ni content on the structure of the carbide material has been studied.

EXPERIMENTAL

Preparation of NiW Bimetallic Oxide Materials

A series of mixed NiW oxide samples were prepared using standard techniques. Nickel nitrate hexahydrate (BDH, >99.99%) was mechanically mixed with tungsten trioxide (Alfa, >99.995%) at Ni/(W + Ni) atomic ratios of 0.1, 0.2, 0.3, 0.4, and 0.5, respectively. The mixtures were ground using a mortar and pestle for 40–60 min, followed by drying at 120°C to give a powder. The dried powder mixture was thoroughly ground for 2 h using a pestle and mortar and then calcined at 650°C in air for 3 h. The mixture was cooled to room temperature and reground into a fine powder. To assist in a uniform distribution of the Ni and W in the mixture, the powder was pressed into pellets and these were

[1] Current address: Johnson Matthey Technology Centre, Blount's Court, Sonning Common, Reading RG4 9NH, U.K.

[2] Current address: BP Chemicals, Chertsey Road, Sunbury on Thames, Middlesex TW16 7LL, U.K.

[3] To whom correspondence should be addressed: Fax: +44-1865-272690. E-mail: malcolm.green@chem.ox.ac.uk.

0021-9517/02 $35.00

placed in a furnace and calcined in air at 650°C for 24 h. The resulting pellets were cooled to room temperature and then pulverized into particles smaller than 250 μm. The resultant oxide samples are labeled $Ni_{0.1}W_{0.9}O_x$, $Ni_{0.2}W_{0.8}O_x$, $Ni_{0.3}W_{0.7}O_x$, $Ni_{0.4}W_{0.6}O_x$, and $Ni_{0.5}W_{0.5}O_x$, corresponding to the calculated Ni/(W + Ni) ratios of 0.1, 0.2, 0.3, 0.4, and 0.5, respectively.

Preparation of Carbide Materials

W and NiW bimetallic carbides were prepared using the TPRe method of Boudard and co-workers (4, 5). A sample of 0.60 g of the mixed oxide was loaded into a 9-mm (o.d.) silica tube plugged with silica wool at both ends. The oxide was reduced under a temperature programme of 1°C/min in a 100 ml/min flow of 20% CH_4/H_2 (volume) to 750°C or 10% C_2H_6/H_2 to 630°C. The reduction was continued at the final temperature until no carbon oxides were detected in the exhaust gas. A GC–MS (Hewlett–Packard 5890A Gas Chromatograph fitted with a Hewlett–Packard 5791A quadruple mass spectrometer detector (MS)) was employed to analyse the gas products during the carburisation process. The m/e mass range at 10–100 was scanned at 1-s intervals, which allowed the gases CO, CO_2, H_2O, CH_4, C_2H_4, and C_2H_6 to be monitored by their parent ions. After carburisation, the sample was cooled to room temperature under Ar by removing the tube from the furnace. Before exposure to air, the samples were passivated in flowing 1.0 vol% O_2/He at room temperature for 5 h. The resultant carbide samples prepared using methane as the carbon source are labeled $Ni_{0.1}W_{0.9}C_x$–M, $Ni_{0.2}W_{0.8}C_x$–M, $Ni_{0.3}W_{0.7}C_x$–M, $Ni_{0.4}W_{0.6}C_x$–M, and $Ni_{0.5}W_{0.5}C_x$–M; those using ethane as the carbon source are labeled $Ni_{0.1}W_{0.9}C_x$–E, $Ni_{0.2}W_{0.8}C_x$–E, $Ni_{0.3}W_{0.7}C_x$–E, $Ni_{0.4}W_{0.6}C_x$–E, and $Ni_{0.5}W_{0.5}C_x$–E.

The structure and components of the mixed oxides and carburised materials were studied by X-ray diffraction (XRD) using a Philips PW1710 diffractometer with Cu$K\alpha$ radiation. The samples were mounted on an aluminum plate with a groove cut into it and smoothed using a microscope slide. Carbon content in the samples was determined by chemical analysis, and the metal content in the samples was measured using the atomic adsorption method. The surface area of each NiW carbide was measured in a homemade glass BET measurement facility using N_2 adsorption.

The morphology of the passivated samples was studied using scanning electron microscopy (SEM) on a Hitachi S-520 microscope operated at 20 kV and 40 mA. The powder sample was dispersed on the specimen stage with acetone.

Raman spectra were recorded in air with a resolution of 2 cm^{-1} using a Yvon Jobin Labram spectrometer with an Ar^+ laser, running in a back-scattered confocal arrangement. The samples were loaded on a microscope slide, smoothed with a slide, and scanned in the range of 90–3000 cm^{-1} with a scanning period of 60 s. To study the effect of the laser on the oxidation of the carbide surface, the passivated sample was loaded in an *in situ* laser Raman cell, which was flushed in Ar for 2 h. The samples were then measured with laser Raman under the same conditions.

Catalyst Activity

The prepared carbide catalysts were tested for the partial oxidation of methane to synthesis gas and for the hydrodenitrogenation of pyridine. The test of catalyst activity for partial oxidation of methane to syngas was carried out by passing a continuous gaseous feed containing pure methane (>99.95%) and air over the catalyst sample (0.2 g) packed in a 9-mm (o.d.) quartz reactor kept in a tubular furnace (i.d., 25 mm). The reactor was heated under flowing Ar or CH_4 to the reaction temperature, and then a well-mixed reactant (CH_4 and air) was conducted to the reactor bed and the pressure was raised to 5 bars. The temperature was measured/controlled by a chromelalumel thermocouple located in the center of the catalyst bed. The reaction temperature could be controlled to within 5°C. The gaseous products were passed to GC–MS through a heated pipeline and analysed by an online gas chromatograph using a spherocarb column. The products were detected with TCD and FID.

For pyridine HDN reaction, the activity tests were made using a 6.4-mm-o.d. silica reactor. Approximately 0.2 g of the catalyst was loaded into the silica reactor and held by silica wool at both ends. The temperature of the catalyst bed was measured by a directly inserted thermocouple. The catalyst sample was heated under H_2 from room temperature to 500°C at a rate of 2°C/min, held at 500°C for 10 h, then cooled to 350°C for further reaction. The reactant (total pressure, ~101 kPa) consisted of flowing H_2 at a rate of 20 cm^3/min saturated with pyridine (99.9%, Aldrich) at 0°C (0.61 kPa), and the gas mixture was passed over the catalyst. The products were separated using a Hayesep D packed column and analysed using a HP 5890 GC equipped with a TCD and FID.

RESULTS AND DISCUSSION

The NiW Bimetallic Oxide Materials

The XRD patterns of the NiW bimetallic oxide materials are shown in Fig. 1. The parent tungsten oxide and the nickel oxide, prepared using the same conditions, were also measured by XRD and the patterns are listed for reference. The main diffraction peaks of WO_3 are seen at 23.1, 23.8, 24.4, and 34.1°. In the XRD pattern of $Ni_{0.1}W_{0.9}O_x$, besides the strong peaks corresponding to WO_3, new peaks at 15.4, 19.1, 25.0, 30.9, and 54.8° are observed. According to Ref. (21), these peaks are attributed to the diffraction of $NiWO_4$. The $NiWO_4$ peak intensity was weaker than WO_3, indicating that the amount of WO_3 is qualitatively greater than $NiWO_4$ in the obtained bimetallic oxide. With increasing Ni content, the peaks due to the diffraction of

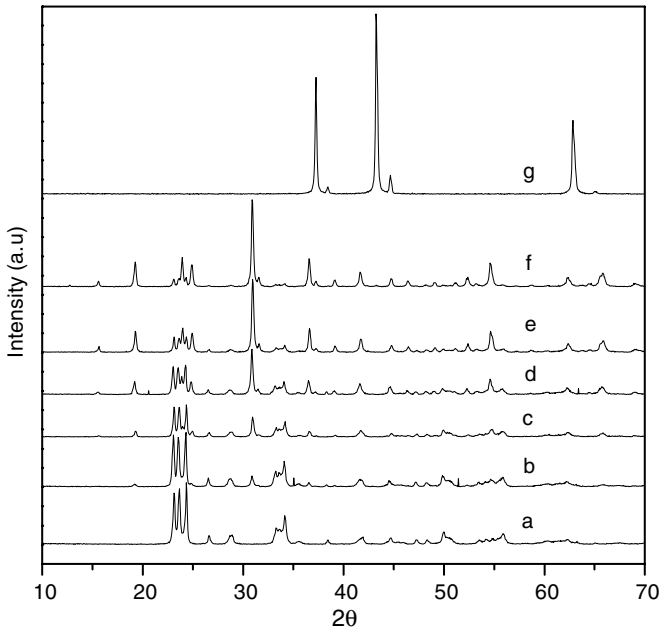

FIG. 1. XRD patterns of the tungsten and NiW bimetallic oxides. (a) WO_3, (b) $Ni_{0.1}W_{0.9}O_x$, (c) $Ni_{0.2}W_{0.8}O_x$, (d) $Ni_{0.3}W_{0.7}O_x$, (e) $Ni_{0.4}W_{0.6}O_x$, (f) $Ni_{0.5}W_{0.5}O_x$, and (g) NiO.

WO_3 become weaker, while those corresponding to $NiWO_4$ become stronger in intensity. This suggests that more and more $NiWO_4$ is formed with the increase of Ni content in the mixture. When the Ni/(Ni + W) atomic ratio is increased to 0.5, the main phase in $Ni_{0.5}W_{0.5}O_x$ is $NiWO_4$, and only a small amount of WO_3 is present. Figure 1g is the XRD pattern of NiO obtained by the decomposition of $Ni(NO_3)_2$ in air, which is a typical XRD pattern of NiO. Comparison of Fig. 1g with other patterns suggests that no pure NiO phase is present in the NiW bimetallic oxides.

The surface vibrational spectrum of the tungsten oxide in the NiW bimetallic oxide materials was measured using laser Raman spectroscopy, and the results are shown in Fig. 2. The Raman spectrum of WO_3 is shown in Fig. 2a. Three main bands, at 276, 714, and 808 cm^{-1}, were observed, which are due to the bending mode, antisymmetric stretch, and symmetric stretch of WO_6 in polycrystalline WO_3. This is in good agreement with the reference results (22). In $Ni_{0.1}W_{0.9}O_x$, the bands due to WO_3 are still quite strong but become broad. This indicates that the surface is mainly covered with WO_3, but its symmetry has been distorted by the presence of NiO. A small band was seen at 897 cm^{-1}, which is the characteristic stretching vibration of short terminal O–W–O bonds: it is confidently assigned to the "totally symmetric" stretching mode of the shortest wolframyl bonds in the unit cell of WO_4 (23). In the samples $Ni_{0.2}W_{0.8}O_x$, $Ni_{0.3}W_{0.7}O_x$, $Ni_{0.4}W_{0.6}O_x$, and $Ni_{0.5}W_{0.5}O_x$, the Raman bands due to the polycrystalline WO_3 decrease in intensity and are broadened, while the typical band of WO_4 at 897 cm^{-1} increases. This indicates that the increase of Ni in the bimetallic oxide yields more $NiWO_4$ on the oxide surface. XRD results of the bimetallic oxides have shown that $NiWO_4$ increases in the bulk NiW bimetallic oxides.

Characterisation of the NiW Bimetallic Carbide Materials Prepared with 20% CH_4/H_2

According to the literature (12, 26), the final temperature for complete phase transition in the carburisation of WO_3 is about 750°C. Hence, in the following NiW bimetallic carbide preparation using 20% CH_4/H_2, the bimetallic oxides were carburised at 1°C/min to 750°C. It was seen that the materials became black in colour after the carburisation. The XRD patterns of the resultant carbides are shown in Fig. 3. The peaks at 38.2, 44.7, and 65.1° are due to the aluminum sample holders. The main peaks are seen at 31.3, 35.5, and 48.4°, which are confidently assigned to the diffraction of WC (fcc NaCl). This is in agreement with the results in Ref. (18). However, some weak peaks appeared at 38.1, 43.4, and 53.2°, which are attributed to the

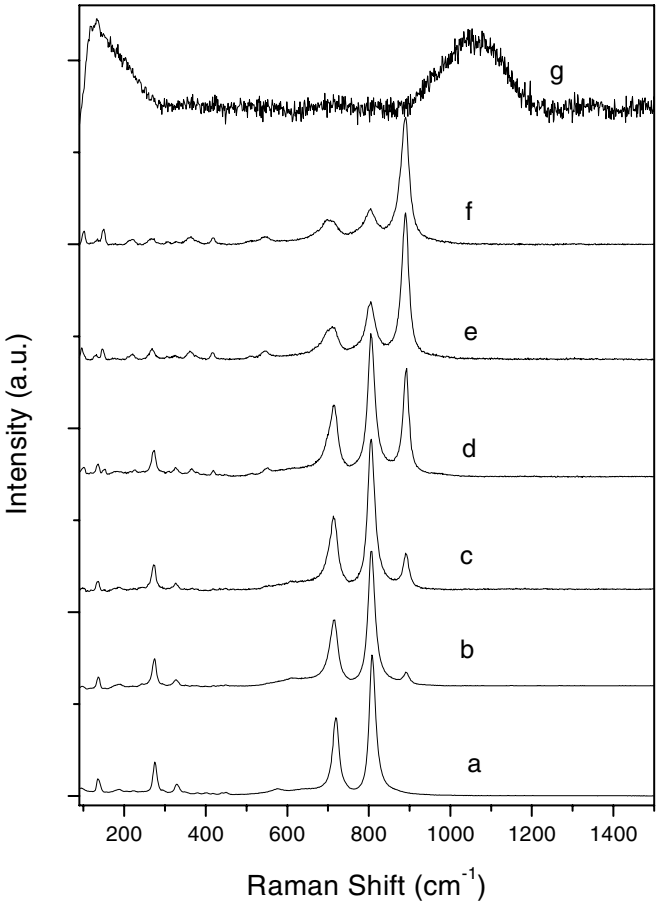

FIG. 2. Laser Raman spectra of the tungsten and NiW bimetallic oxides. (a) WO_3, (b) $Ni_{0.1}W_{0.9}O_x$, (c) $Ni_{0.2}W_{0.8}O_x$, (d) $Ni_{0.3}W_{0.7}O_x$, (e) $Ni_{0.4}W_{0.6}O_x$, (f) $Ni_{0.5}W_{0.5}O_x$, and (g) NiO.

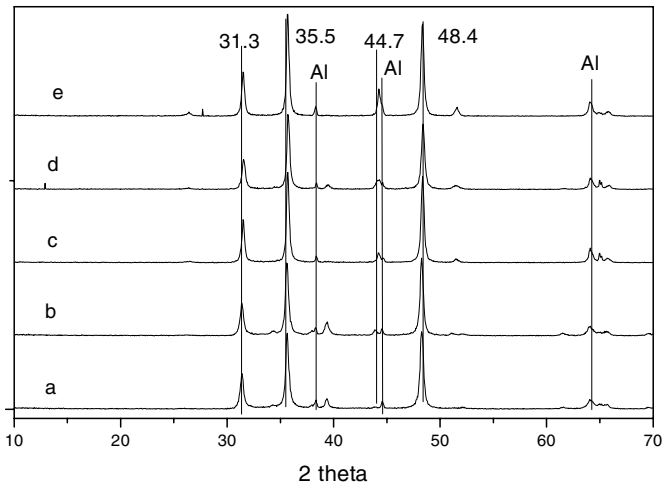

FIG. 3. XRD patterns of the NiW bimetallic carbide prepared using 20% CH_4/H_2. (a) $Ni_{0.1}W_{0.9}C_x$, (b) $Ni_{0.2}W_{0.8}C_x$, (c) $Ni_{0.3}W_{0.7}C_x$, (d) $Ni_{0.4}W_{0.6}C_x$, and (e) $Ni_{0.5}W_{0.5}C_x$.

diffraction of Ni metal in the samples. These peaks become more intense with the increase in Ni content, suggesting more nickel metal is separated from the $NiWO_4$ during the carburisation with 20% CH_4/H_2. These results suggest that the $NiWC_x$ carbides prepared using CH_4/H_2 are not composed of a homogeneous phase, as Ni metal and WC carbide are present in the materials. This is in agreement with the results of Oyama *et al.* in preparing NiWOC with CH_4/H_2 at 973 K (18). With the increase of Ni content in the NiW bimetallic carbides, the diffraction peaks of the bimetallic carbides become broader, indicating that the crystallite size becomes smaller in these carbided materials. In $Ni_{0.3}W_{0.7}C_x$–*M*, $Ni_{0.4}W_{0.6}C_x$–*M*, and $Ni_{0.5}W_{0.5}C_x$–*M*, a small peak at 26.6° was present in the XRD patterns, which is characteristic of the formation of graphitic carbon in the carbide. The peak becomes stronger with the increasing Ni/(Ni + W) ratio, suggesting that more carbon deposition occurs in the materials containing more Ni metal. This is because Ni metal facilitates the decomposition of methane to its elements (24).

The passivated $NiWC_x$–*M* materials were measured using laser Raman spectroscopy in air at room temperature, and the spectra are shown in Fig. 4. In $Ni_{0.1}W_{0.9}C_x$ three broad and unsymmetrical bands were seen in the range of 600–900 cm^{-1}, which are characteristic bands of WO_3 (688 and 811 cm^{-1}) and WO_4 (884.2 cm^{-1}). This indicates that the surface of the carbide is reoxidised, although XRD measurements show that the main phase is still that of carbide in $Ni_{0.1}W_{0.9}C_x$. The oxidation may come from the passivation process or as a consequence of laser heating during the measurement. To identify the cause of the surface oxidation of the carbide, the same sample was mounted in a silica cell flushed with Ar and measured *in situ*. The same spectrum as with a sample measured in air was obtained. This suggests that the surface oxidation results from the passivation process. However, the peak (884.2 cm^{-1}) due to the $NiWO_4$ is much stronger than in $Ni_{0.1}W_{0.9}O_x$, suggesting that more $NiWO_4$ is distributed on the surface of $Ni_{0.1}W_{0.9}C_x$. This is probably because $NiWC_x$ is more sensitive to O_2 than WC or because the $NiWO_4$ phase migrates to the surface during the carburisation and passivation. Very small peaks at 1342 and 1571.5 cm^{-1} were also seen in the Raman spectrum of $Ni_{0.1}W_{0.9}C_x$–*M*, and these are assigned as the D and G vibrations of carbon deposited in the catalyst. The laser Raman spectrum of $Ni_{0.2}W_{0.8}C_x$–*M* is shown in Fig. 5b. The peaks due to WO_3 and $NiWO_4$ become weak, while the peaks of the carbon deposition become more intense. This shows that increase of Ni content in the oxide leads to more carbon deposition. Further increasing the Ni content has no effect on the surface of the carbide after carburisation and passivation. The main Raman band of $Ni_{0.3}W_{0.7}C_x$–*M*, $Ni_{0.4}W_{0.6}C_x$–*M*, and $Ni_{0.5}W_{0.5}C_x$–*M* is seen at 884.2 cm^{-1}, together with two small peaks, at 688 and 811 cm^{-1}. This is similar to the Raman spectrum of $Ni_{0.5}W_{0.5}O_x$, suggesting that carburisation with CH_4/H_2 and passivation results in the formation of $NiWO_4$ at the carbide surface. The peaks at 1342 and 1571 cm^{-1} also become more intense with increasing Ni content, indicating more carbon deposition is formed in the carbide when carburised with CH_4/H_2 to 750°C.

The SEM images of the carbide particles prepared using CH_4/H_2 are shown in Fig. 5. The overall morphologies of the NiW bimetallic carbides are irregular, and the surfaces of the particles are very rough. The catalyst seems to consist of different phases. One is the WC, another is $NiWC_x$, and the black particles on the surface are probably nickel metal. In the SEM micrograph of $Ni_{0.1}W_{0.9}C_x$–*M*, the surface black dots, e.g., nickel particles, are very small. With an increase in nickel concentration, the Ni particles in the NiW bimetallic carbides become larger, and the separation

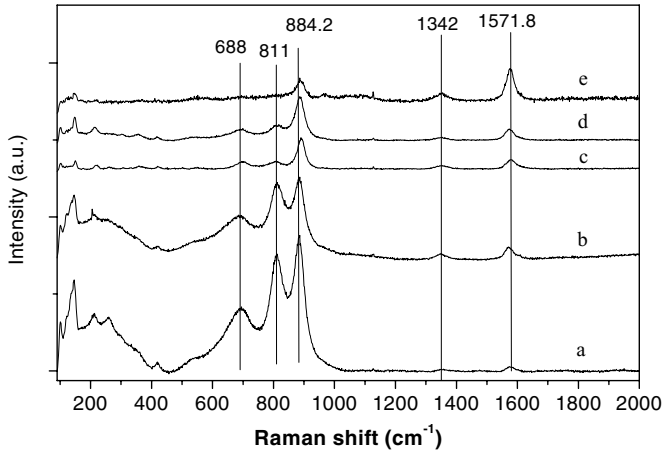

FIG. 4. Laser Raman spectra of the NiW bimetallic carbide prepared using 20% CH_4/H_2. (a) $Ni_{0.1}W_{0.9}C_x$, (b) $Ni_{0.2}W_{0.8}C_x$, (c) $Ni_{0.3}W_{0.7}C_x$, (d) $Ni_{0.4}W_{0.6}C_x$, and (e) $Ni_{0.5}W_{0.5}C_x$.

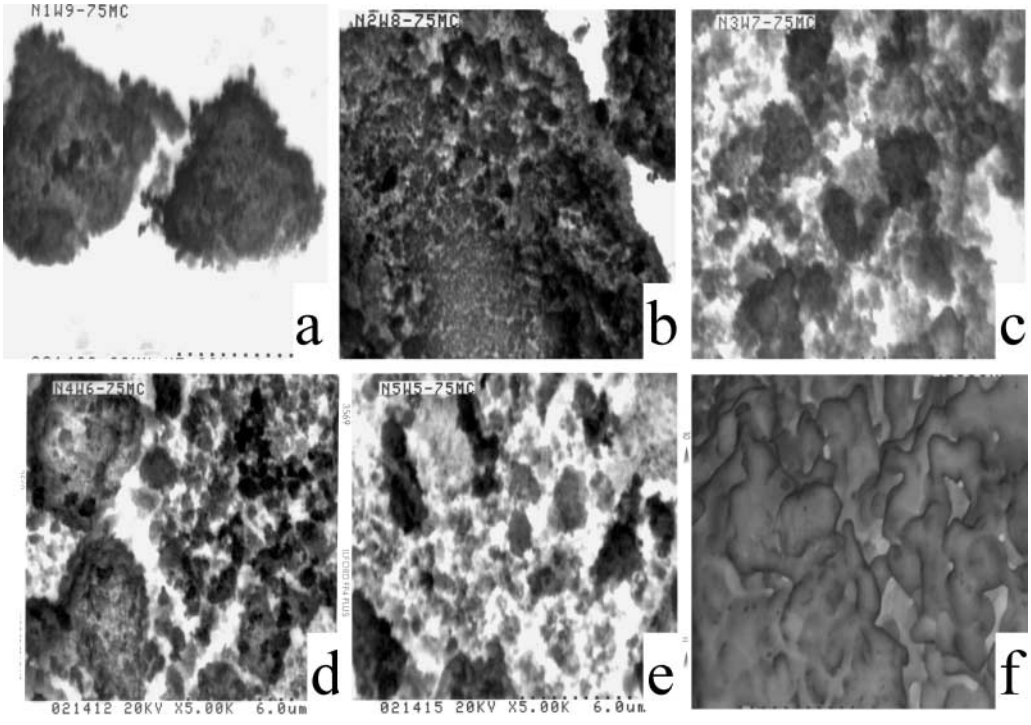

FIG. 5. SEM graphs of NiW bimetallic carbides prepared with 20% CH_4/H_2 at Ni/(W + Ni) ratios of (a) 0.1, (b) 0.2, (c) 0.3, (d) 0.4, (e) 0.5, and (f) 1.0.

between Ni particles and WC and $NiWC_x$ becomes clearer, suggesting that carburisation of $NiWO_x$ with 20% CH_4/H_2 leads to more phase separation with an increase in Ni content in the oxides. However, when NiO is carburised with 20% CH_4/H_2 to 750°C, the SEM images of the resultant materials show porous and partially sintered nickel metal ("nickel sponge"), which has a totally different appearance from the nickel particles distributed in $NiWC_x$.

Characterisation of the NiW Bimetallic Carbide Materials Prepared with 10% C_2H_6/H_2

Previous study has shown that when using ethane as the carburising agent, the temperature for complete phase transformation from WO_3 to W_2C is around 630°C (12, 26). Hence in this work, we carburised the NiW series of oxides with 10% C_2H_6/H_2 at a rate of 1°C/min up to 630°C and held it at the final temperature for 2 h. The XRD patterns of the $NiWC_x$ prepared using ethane are shown in Fig. 6. The main diffraction peaks, at 35.02, 38.5, and 39.6°, in Fig. 6a are assigned to W_2C (26), suggesting that the main phase in the resultant material is W_2C (Pbcn). However there is still a small peak at 26.0°, the characteristic peak of WO_2 (27), which may come from the oxidation of W_2C during the passivation or the incomplete carburisation process. When Ni is added to WO_3 to form $Ni_{0.1}W_{0.9}O_x$ and carburised with 10% C_2H_6/H_2, the diffraction peaks of the W_2C become sharper, with no peaks corresponding to Ni metal being detected, suggesting that the nickel metal has either entered the lattice of W_2C or is highly dispersed on the carbide, which is undetectable by X-ray diffraction. However the peak due to WO_2 is still present, indicating that only some of the WO_3 is converted to WO_2 during the carburisation. Carburising $Ni_{0.2}W_{0.8}O_x$ with 10% C_2H_6/H_2 gives rise to sharper diffraction peaks of W_2C, and the peaks due to Ni metal are still not observed. This suggests that the crystal size of W_2C continues to increase and that the Ni is highly dispersed or enters the lattice of the W_2C. For

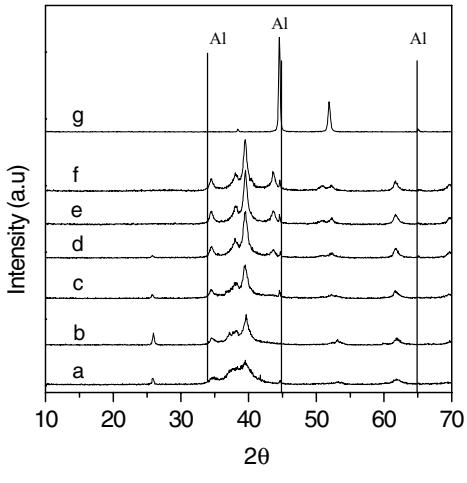

FIG. 6. XRD pattern of Ni and W bimetallic carbides reduced with 10% C_2H_6/H_2. (a) W_2C, (b) $Ni_{0.1}W_{0.9}C_x$, (c) $Ni_{0.2}W_{0.8}C_x$, (d) $Ni_{0.3}W_{0.7}C_x$, (e) $Ni_{0.4}W_{0.6}C_x$, (f) $Ni_{0.5}W_{0.5}C_x$, and (g) NiC_x.

the $Ni_{0.2}W_{0.8}O_x$ sample, the peaks due to WO_2 became much weaker, indicating that the presence of more Ni in the NiW oxide promotes the conversion of oxide to carbide. In $Ni_{0.3}W_{0.7}C_x$–*E*, the peaks due to W_2C became further sharpened, and the peaks due to WO_2 almost disappeared. But a peak was observed at 43.2°, and this is assigned to the diffraction of Ni metal. This suggests that the increase of Ni favours the phase transformation of WO_3 to carbide; the excess Ni metal separates from the lattice of $NiWC_x$ or forms large particles. $Ni_{0.4}W_{0.6}C_x$–*E* and $Ni_{0.5}W_{0.5}C_x$–*E* have the largest crystallite size among those in the $NiWC_x$–*E* series and the highest content of nickel metal. WO_2 is absent in the resultant bimetallic carbide, suggesting that the presence of Ni catalyses the carburisation of WO_3. A sample of pure NiO was also carburised with 10% C_2H_6/H_2 to 630°C; the XRD patterns of this material are shown in Fig. 6g. Three peaks due to Ni metal were seen, but no Ni_3C (28) was observed. This shows that NiO is reduced to Ni metal by the carburising medium.

The laser Raman spectra of the NiW carbides prepared using 10% C_2H_6/H_2 are shown in Fig. 7. The sample of WC_x–*E* has Raman bands at 250, 684, and 793 cm^{-1}, which are assigned to the Raman mode of WO_3. This indicates that the surface of W_2C–*E* has changed back to the oxide during the passivation procedure. Comparison of Figs. 7a and 2a shows that the Raman bands become much broader but the bands are of similar wavelength, suggesting that the surface symmetry of the WO_3 in W_2C is somewhat distorted during the carburisation and passivation. The Raman mode of $Ni_{0.1}W_{0.9}C_x$–*E* is very similar to its oxide precursor, but different from the $Ni_{0.1}W_{0.9}C_x$–*M*, suggesting that the carburisation with ethane and then passivation does not change the overall surface symmetry of $Ni_{0.1}W_{0.9}O_x$. This may give some evidence that the carburisation with ethane to carbide is a pseudomorphic process (12). In the Raman spectrum of $Ni_{0.2}W_{0.8}C_x$–*E*, the peaks corresponding to $NiWO_4$ grow more intense than those in $Ni_{0.1}W_{0.9}C_x$–*E*, although the main phase at the surface is still WO_3, which is similar to the $Ni_{0.1}W_{0.9}C_x$–*M* sample. In the Raman spectrum of $Ni_{0.3}W_{0.7}C_x$–*E*, the band due to $NiWO_4$ (883 cm^{-1}) becomes the strongest peak, suggesting that the main component on the carbide surface is $NiWO_4$. This is different from its starting oxide, indicating that the carburisation of $Ni_{0.3}W_{0.7}O_x$ with ethane leads to the formation of more $NiWO_4$ in the surface. With the increase in nickel content to 0.4 and 0.5 in the bimetallic carbides, the amount of WO_3 in the passivated carbide samples further decreases, and the main surface phase becomes $NiWO_4$ in the passivated samples: this is different from the corresponding starting oxides. The results also show that the carburisation process helps the formation of $NiWO_4$ in the bimetallic surface. Comparison of Figs. 7 and 4 shows that no Raman peaks at 1342 and 1571 cm^{-1} are observed in the NiW bimetallic carbides prepared with ethane. This indicates that carburisation with ethane to 630°C does not lead to carbon deposition over the carbide materials.

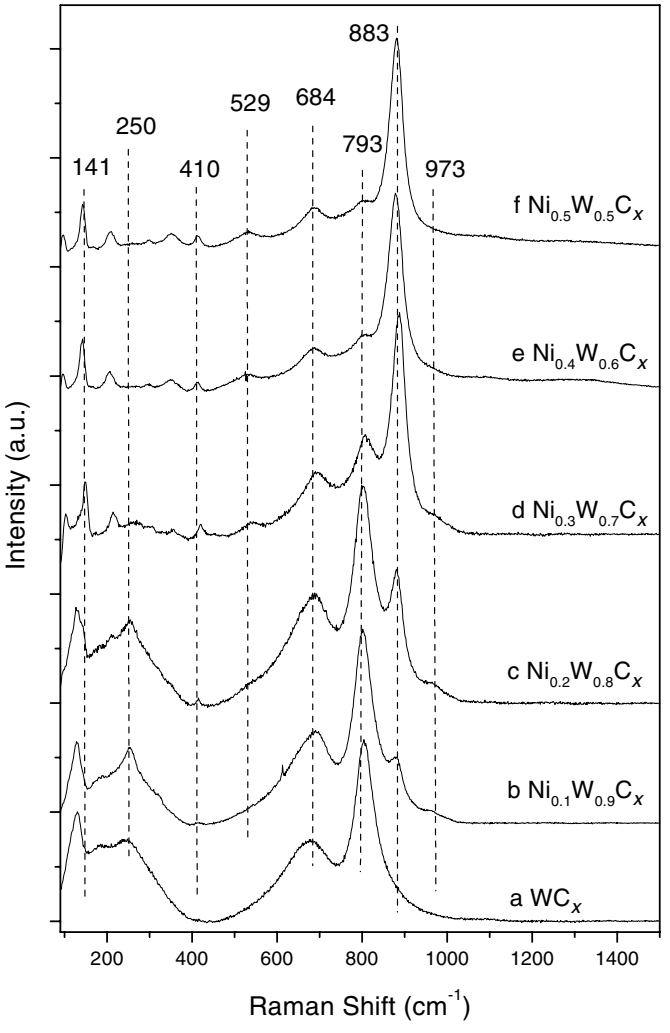

FIG. 7. Laser Raman spectra of the NiW bimetallic carbide prepared using 10% C_2H_6/H_2.

The SEM micrographs of $NiWC_x$–*E* are given in Fig. 8. The morphology of $Ni_{0.1}W_{0.9}C_x$–*E* is irregular, and the surface is not as rough as that $Ni_{0.1}W_{0.9}C_x$–*M*. The average particle size is ca. 3–5 μm, almost the same as that of $Ni_{0.1}W_{0.9}O_x$. The morphology of $Ni_{0.2}W_{0.8}C_x$–*E* is different from that of $Ni_{0.2}W_{0.8}C_x$–*M* and $Ni_{0.2}W_{0.8}O_x$; the size ranges from 2 to 5 μm. When the percentage of nickel is increased to 0.3, the surface of $Ni_{0.3}W_{0.7}C_x$–*E* becomes much rougher, and the particles are loosely aggregated. More black particles are present in $Ni_{0.4}W_{0.6}C_x$–*E* (Fig. 8d) (which are attributed to $Ni_{(m)}$) and the surface is consistently very rough. In $Ni_{0.5}W_{0.5}C_x$–*E*, the surface black particles become larger.

The changes of carbon content and particles size of the $NiWC_x$ prepared with methane and ethane are shown in Fig. 9. The carbon content in W_2C is 3.72 wt% for W_2C–*M*

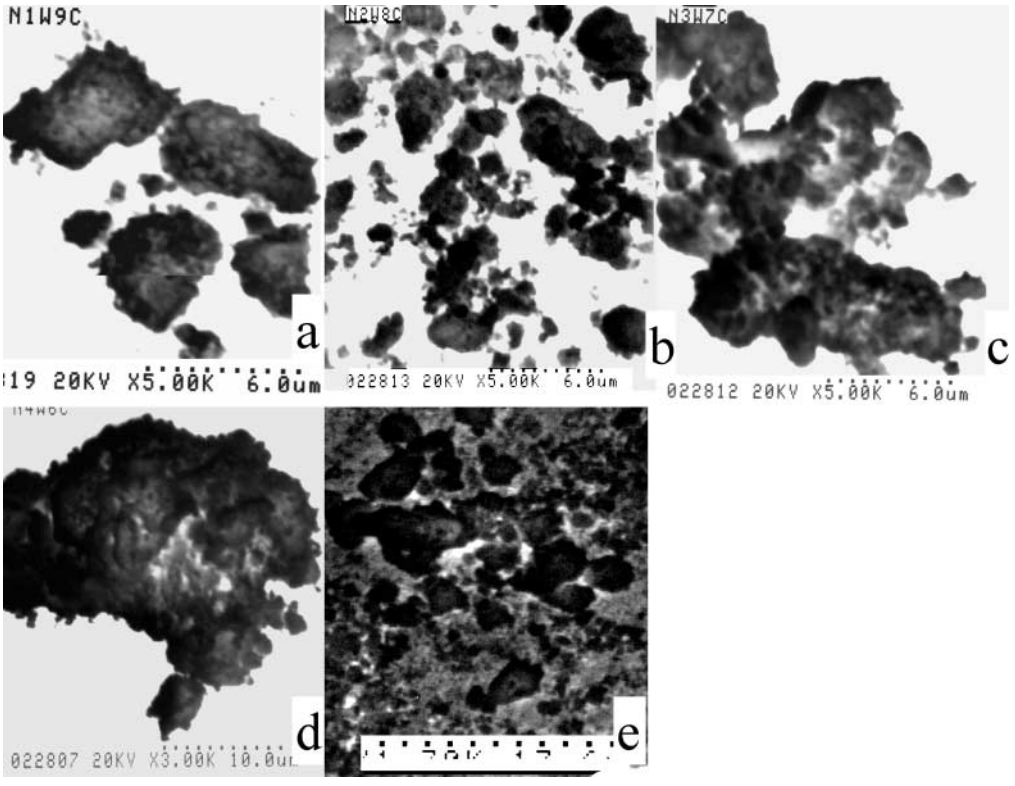

FIG. 8. SEM graphs of NiW bimetallic carbides prepared with 10% C_2H_6/H_2 with Ni/(W + Ni) ratios of (a) 0.1, (b) 0.2, (c) 0.3, (d) 0.4, and (e) 0.5.

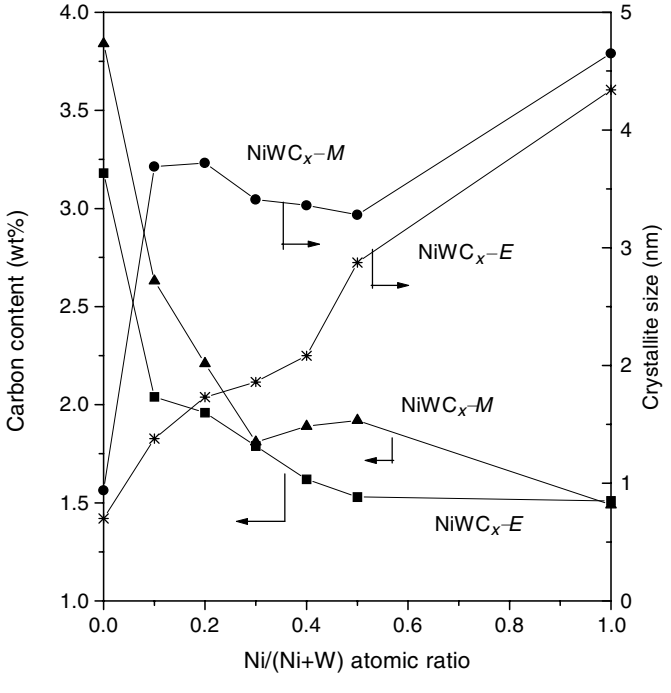

FIG. 9. Change in carbon content and particle size with the ratio of Ni/W in the carbide.

and to 3.2 wt% for W_2C–*E*. The carbon content decreases rapidly to 2.66 wt% for $Ni_{0.1}W_{0.9}C_x$–*M* and to 2.05 wt% for $Ni_{0.1}W_{0.9}C_x$–*E*. As the nickel content increases in the carbides, the $NiWC_x$ contains less carbon in the carbides, indicating that carbon is mainly bonded with tungsten in the bimetallic carbides and Ni is present in the form of metallic states. The carbon content in NiO carburised with methane and ethane is almost the same, ca. 1.53 wt%. The XRD result in Fig. 6 shows that Ni is in the metallic state; hence it is inferred that the carbon in the carburised NiO is carbon deposit.

The size of the W_2C crystallites has been calculated by the X-ray diffraction peak [220] at 38.9°. The crystallite size of the $Ni_{0.1}W_{0.9}C_x$–*M* is calculated as 3.8 nm, larger than W_2C–*M* (0.95 nm). The $Ni_{0.2}W_{0.8}C_x$–*M* has almost the same crystallite size as $Ni_{0.1}W_{0.9}C_x$–*M*, but the carbide crystallites become smaller with an Ni content increase in $Ni_{0.3}W_{0.7}C_x$–*M*, $Ni_{0.4}W_{0.6}C_x$–*M*, and $Ni_{0.5}W_{0.5}C_x$–*M*. A significant difference in crystallite size is present among the carbides prepared with ethane. W_2C–*E* has the smallest crystallite size (0.78 nm) among the ethane-derived carbides. The crystallite size increases to 1.15 nm for $Ni_{0.1}W_{0.9}C_x$ and gradually grows to 1.78 nm with increasing nickel content up to 0.4. In $Ni_{0.5}W_{0.5}C_x$–*E*, the crystallite size of the carbide is around 2.68 nm. This shows that increasing Ni content in the precursors leads to a larger crystallite size distribution of W_2C.

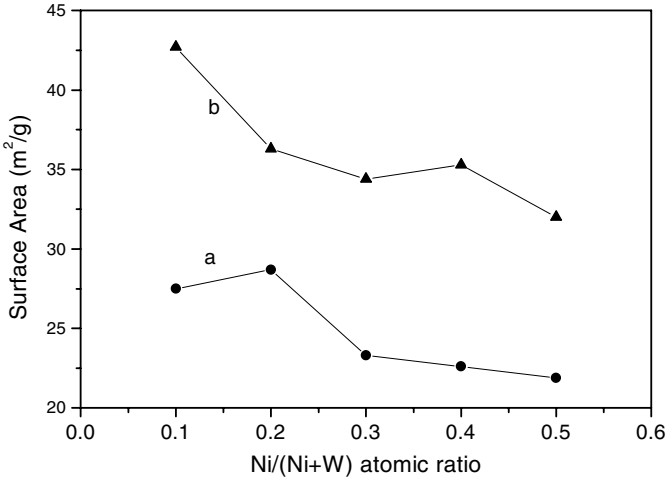

FIG. 10. Changes in surface area of NiW bimetallic carbides with Ni/(Ni + W) ratio. Carbide prepared using (a) 20% CH_4/H_2 and (b) 10% C_2H_6/H_2.

The dependence of surface area on the percentage of nickel content in the NiW bimetallic carbides is shown in Fig. 10. The surface area is 25 m^2/g for $Ni_{0.1}W_{0.9}C_x$–*M*, and 27 m^2/g for $Ni_{0.2}W_{0.8}C_x$–*M*. It decreases to 23 m^2/g when the nickel content is 0.3. No significant changes occur in the surface area of $Ni_{0.4}W_{0.6}C_x$–*M* and $Ni_{0.5}W_{0.5}C_x$–*M*. In the case of the NiW bimetallic carbides prepared with ethane, $Ni_{0.1}W_{0.9}C_x$–*E* has a surface area of 45 m^2/g. As the nickel content increases in the materials, the surface area decreases more rapidly for the ethane-derived materials than it does for those prepared from methane. However, in general the surface areas of the NiW carbides prepared with ethane are still larger than for methane since the temperature of formation is lower. This can be explained by the formation of smaller carbide particles when ethane is used as the carburising agent.

Monitoring of the Carburisation of $NiWO_x$ with 10% C_2H_6/H_2 Using Online GC

It has been shown that ethane is a useful agent for the carbide preparation (3, 29, 30). Direct monitoring of the carburisation process may provide some information on the carburisation process.

The changes of product distribution during the carburisation of WO_3 with 10% C_2H_6/H_2 are shown in Fig. 11a. CO starts to be produced at 565°C, along with the production of methane and a decrease in C_2H_6 and H_2. But the temperature for complete consumption of ethane is 630°C, while CO yield is almost constant during the carburisation after 630°C. This suggests that WO_3 could be carburised above 565°C. Some of the ethane decomposes into methane as the WO_3 is converted to carbide, and the carburisation process is not complete until 630°C. The changes in the backpressure of the reactor during the carburisation can reflect changes in the surface area of the materials. Generally speaking, a decrease in the backpressure indicates the formation of a more porous material and thus a higher surface area. The backpressure of the reactor in the carburisation of WO_3 did not decrease until 450°C, corresponding to a small decrease in H_2 but no changes in C_2H_6, suggesting that the surface area of WO_3 is first increased by its reduction to WO_2 by H_2. However, the backpressure increases after C_2H_6 takes part in the reduction of WO_3. This may be explained by the carbon deposition in the reactor or the transformation from higher surface area materials to more condensed materials by further carburisation and sintering.

Figure 11b shows the product distribution and backpressure changes during the carburisation of $Ni_{0.1}W_{0.9}O_x$. Ethane and hydrogen start to decrease at 404°C, corresponding to the yield of a small amount of CO, suggesting that ethane and hydrogen take part in the reduction and carburisation of $Ni_{0.1}W_{0.9}O_x$ at the same time. It is interesting to see that the amount of ethane unconverted decreases until 475°C and then increases again from 475 to 510°C. The ethane is completely converted to CH_4 and CO above this temperature. The production of CO stopped after the carburisation had been held at 630°C for 100 min. These results show that the ethane and hydrogen take part in the first-stage reduction and carburisation simultaneously. A transition state of $Ni_{0.1}W_{0.9}O_x$ suppresses the hydrogenolysis of ethane, because the ethane concentration was seen to increase after the first-stage reduction and carburisation. The presence of Ni in the oxide helps to decrease the carburisation temperature. The backpressure of the reactor first increased with rising temperature, but decreased after 505°C, suggesting that the surface area is mainly formed by the reduction of the oxide with ethane rather than hydrogen. This is different from the carburisation of monometallic oxides (29).

Increasing the Ni content in the $NiWO_x$ further decreased the temperature at which ethane and hydrogen become active in the reduction and carburisation of $NiWO_x$. Ethane and hydrogen first reacted with $Ni_{0.2}W_{0.8}O_x$ at 398°C, and with $Ni_{0.3}W_{0.7}O_x$ at 372°C (Figs. 11c and 11d). The temperature for the production of the transition phase, which suppresses the hydrogenolysis of ethane, is 460°C in the two oxides. The reactor backpressure during the carburisation of $Ni_{0.2}W_{0.8}O_x$ continued to decrease after 502°C, after which ethane was rapidly converted to methane. But for $Ni_{0.3}W_{0.7}O_x$, the reactor backpressure during the carburisation decreased rapidly after 530°C, at which point ethane was completely converted to CH_4 and CO, and it increased again after 620°C. After the carburisation had been held at 630°C for 90 min, the backpressure decreased again. This suggests that $Ni_{0.3}W_{0.7}O_x$ is first converted into a porous material but in one of the intermediate states is a more sintered material. Further carburisation causes an increase in the subsequent surface area of the material.

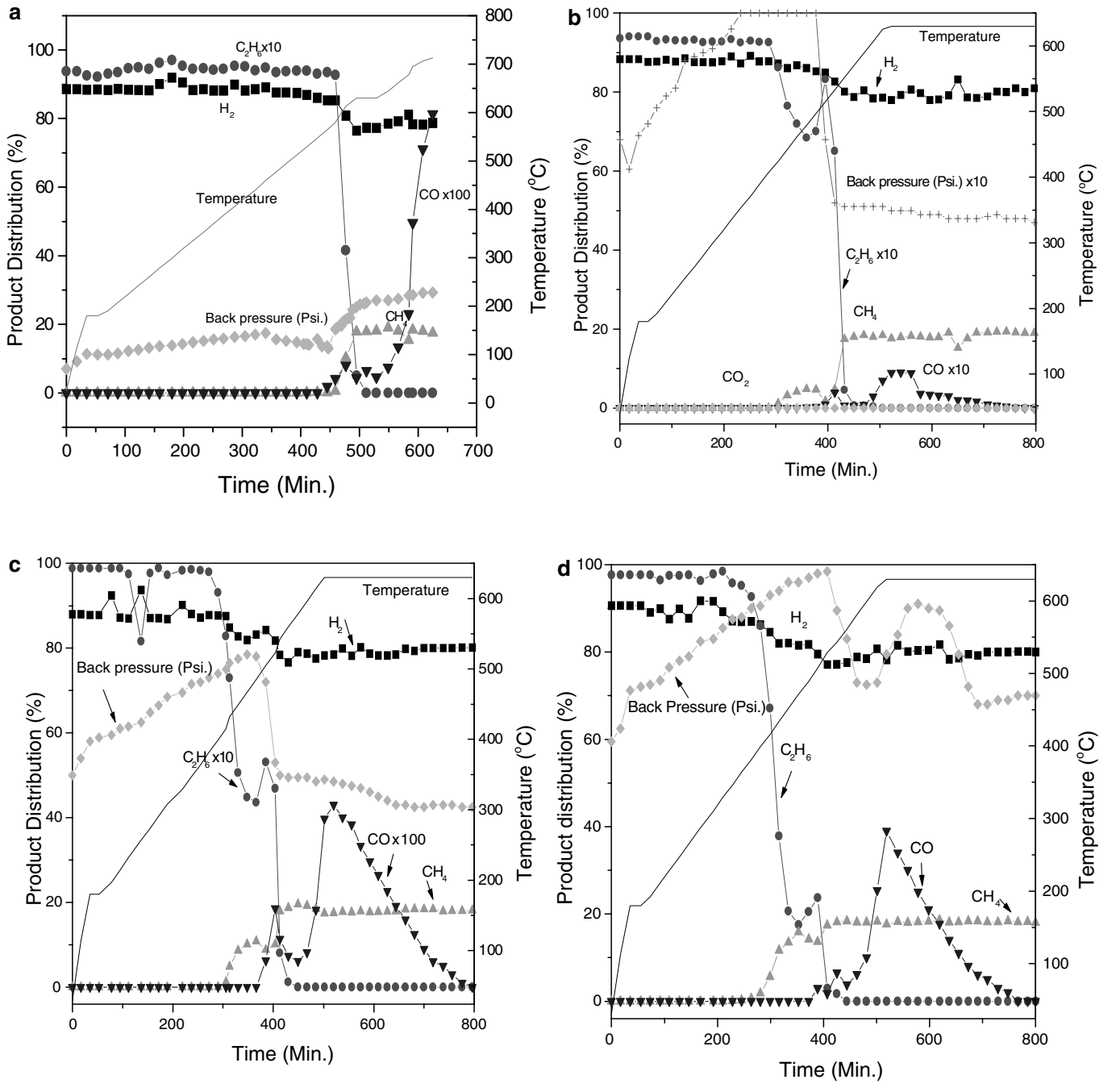

FIG. 11. Product distribution and back pressure change during temperature-programmed carburisation with 10% C_2H_6/H_2. (a) WO_3, (b) $Ni_{0.1}W_{0.9}O_x$, (c) $Ni_{0.2}W_{0.8}O_x$, (d) $Ni_{0.3}W_{0.7}O_x$, (e) $Ni_{0.4}W_{0.6}O_x$, (f) $Ni_{0.5}W_{0.5}O_x$, and (g) NiO.

The temperature for the first-stage reduction and carburisation of $Ni_{0.4}W_{0.6}O_x$ decreases to 300°C, and after the ethane is rapidly converted to CH_4. However, no CO or CO_2 is produced before 498°C, suggesting that the partly reduced $Ni_{0.4}W_{0.6}O_x$ catalyses the methanation of the ethane. Ethane starts to recover after 498°C, corresponding to the production of CO and a sharp increase in backpressure, which starts to decrease after ethane is involved in the carburisation at 570°C. This suggests that the carburisation intermediates formed from $Ni_{0.4}W_{0.6}O_x$ suppress the hydrogenolysis of ethane; further reaction with ethane gives rise to a high surface area material. As CO and even CO_2 continues to be produced, the backpressure of the reactor continues to decrease, suggesting that the surface area of the carburised material is formed during carburisation. The temperature for the hydrogenolysis of ethane to methane over $Ni_{0.5}W_{0.5}O_x$ is 382°C, which is higher than the $NiWO_x$ oxides containing less Ni, and the backpressure starts to

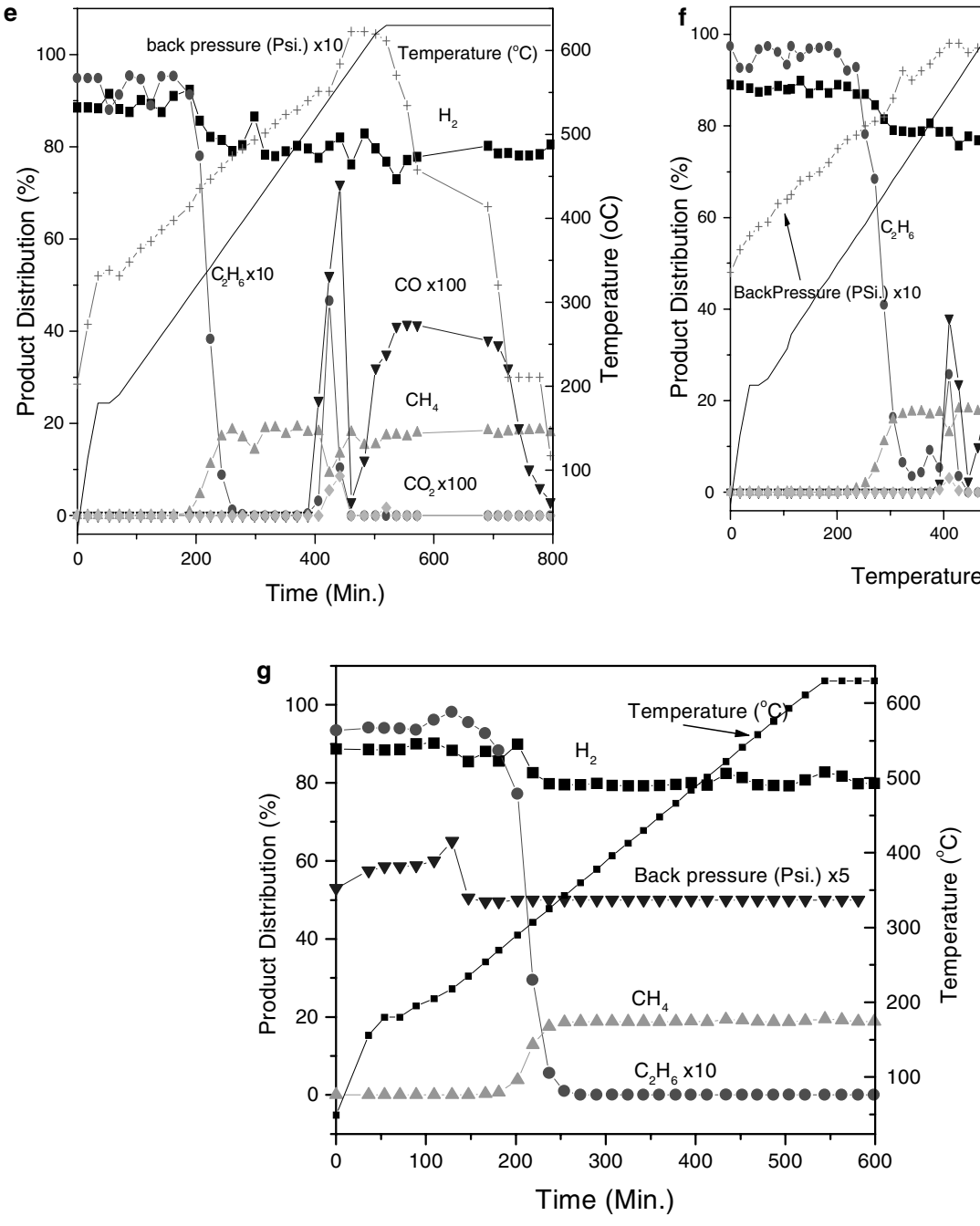

FIG. 11—*Continued*

decrease after the occurrence of the second CO production peak. This indicates that the behaviour of the carburisation of $Ni_{0.5}W_{0.5}O_x$ is different from the other bimetallic oxides. This is shown in Fig. 1; the $Ni_{0.5}W_{0.5}O_x$ is mainly composed of $NiWO_4$.

The changes in the carburising agent and the product distribution for the carburisation of NiO are shown in Fig. 11g. Ethane is methanated at 275°C, which is a lower temperature than the $NiWO_x$ systems. The only product is CH_4 during the carburisation, and the backpressure is constant after 250°C. Apparently the carburisation process of $NiWO_x$ systems is different from either NiO or WO_3, suggesting that Ni in the $NiWO_x$ is not present as a separate phase.

Decker *et al.* (3) studied the preparation of bulk tungsten carbide with C_2H_6/H_2 and found that the carburisation process was related to the composition of the carburising agent. The temperature for the WC carbide formation using C_2H_6/H_2 was about 750°C, while the temperature for WC preparation using CH_4/H_2 was 150°C higher than for

TABLE 1

Activity and Stability of $NiWC_x$ Carbide Catalyst for Partial Oxidation of Methane under Atmospheric Pressure Conditions[a]

Catalysts	$Ni_{0.1}W_{0.9}C_x$	$Ni_{0.2}W_{0.8}C_x$	$Ni_{0.3}W_{0.7}C_x$	$Ni_{0.4}W_{0.6}C_x$	$Ni_{0.5}W_{0.5}C_x$
CH_4 conversion[b]	85.0%	87.1%	88.5%	88.6%	86%
CO selectivity	84%	88%	92%	92%	93%
H_2/CO volume ratio	1.87	1.96	2.01	2.02	2.1
Catalyst life time[c] (h)	2.2	4.6	7.2	16.7	24

[a] Reaction conditions: T, 800°C; P, 1 bar; GHSV, 12,000 h^{-1}; $CH_4/O_2 = 2$. Air is used as the oxidant.
[b] CH_4 conversion refers to the conversion of CH_4 at the initial reaction.
[c] The lifetime of the catalyst refers to the period between the start of the initial reaction and the point at which the catalytic activity starts to drop.

C_2H_6/H_2. This is the reason for carburising $NiWO_x$ to 750°C when using methane as the carburising agent. When Ni was added to WO_3, it was seen that, using 10% C_2H_6/H_2 as the carburising agent, the complete phase transformation temperature was lowered significantly. The main CO emission peak appeared at 600°C and when held at 630°C for 2 h, the emission of CO was completed. After the temperature holding, further increase in the carburising temperature did not lead to the emission of more CO from the carburisation using 10% C_2H_6/H_2, suggesting that the carburisation of $NiWO_x$ with 10% C_2H_6/H_2 is complete at 630°C.

Catalytic Activity Tests of the NiW Bimetallic Carbide Catalysts

The catalytic activities of the bimetallic carbide catalysts were tested for the reactions of partial oxidation of methane and hydrodenitrogenation. In the partial oxidation of methane to synthesis gas, the catalysts were first heated to 800°C under flowing Ar, and then the reactants of methane and air was introduced to the reactor at the 800°C. It is seen that the NiW bimetallic carbide catalysts prepared with CH_4/H_2 and C_2H_6/H_2 had a similar performance for this reaction, which may be due to the reaction at the temperature higher than the carburisation temperatures. Hence here we only list the results of $NiWC_x$–M. As shown in Table 1, under atmospheric pressure, $Ni_{0.1}W_{0.9}C_x$ showed the lowest CH_4 conversion and H_2/CO ratio. The catalyst activity dropped after 2 h of time on stream. With the Ni content increased from 0.1 to 0.4 in the NiW bimetallic carbides, the CH_4 conversion gradually increased to 88.6%, and catalyst lifetime was prolonged to 16.7 h. The H_2/CO ratio also increased to 2.02. These results suggest that increase of the Ni content in the bimetallic carbide catalysts help to improve the catalyst stability and activity. XRD and laser Raman data (not shown here) of the postreaction catalysts indicated that WO_3 and WO_2 were produced in the postreaction catalysts. The high activity and stability shows that Ni metal itself is an active component for the reaction. However, when Ni content was increased to 0.5 in $NiWC_x$, CH_4 conversion decreased to 86%, but the catalyst selectivity and stability improved significantly. The catalyst was stable over 24 h of time on stream. The high stability of $Ni_{0.5}W_{0.5}C_x$ is due to the high Ni content. The high H_2/CO ratio (2.1) suggests that methane decomposition occurs over the catalysts. This may help to improve the stability of the WC under the reaction conditions.

When the pressure for the methane partial oxidation reaction was raised to 4 bars, methane conversion and CO selectivity over all the NiW bimetallic carbide catalysts were about 85 and 93%, respectively, while the H_2/CO ratio increased with the increase in nickel content (Table 2).

TABLE 2

Activity and Stability of $NiWC_x$ Carbide Catalyst for Partial Oxidation of Methane to Synthesis Gas under Pressure Conditions[a]

Catalysts	$Ni_{0.1}W_{0.9}C_x$	$Ni_{0.2}W_{0.8}C_x$	$Ni_{0.3}W_{0.7}C_x$	$Ni_{0.4}W_{0.6}C_x$	$Ni_{0.5}W_{0.5}C_x$
CH_4 conversion[b]	85.7%	84.6%	85.1%	86.2%	84.6%
CO selectivity	92.1%	93.0%	92%	92%	93%
H_2/CO volume ratio	1.98	1.99	2.04	2.06	2.2
Catalyst life time[c] (h)	24	24	24	24	24

[a] Reaction conditions: T, 800°C; P, 4 bar; GHSV, 12,000 h^{-1}; $CH_4/O_2 = 2$. Air is used as the oxidant.
[b] CH_4 conversion refers to the conversion of CH_4 at the initial reaction.
[c] The lifetime of the catalyst refers to the period between the start of the initial reaction and the point at which the catalytic activity starts to drop. In this test, all the catalysts are active and no activity drops during the 24 h of reaction.

TABLE 3

Activity of $NiWC_x$ Carbide Catalysts for Pyridine Hydrodenitrogenation[a]

Catalysts	$Ni_{0.1}W_{0.9}C_x$	$Ni_{0.2}W_{0.8}C_x$	$Ni_{0.3}W_{0.7}C_x$	$Ni_{0.4}W_{0.6}C_x$	$Ni_{0.5}W_{0.5}C_x$
Pyridine conversion[b]	45.7%	65.4%	75.1%	62.1%	59.3%
Pyridine conversion[c]	62.0%	78.3%	84.1%	88.6%	80.5%

[a] Reaction conditions: T, 350°C; P, 1 bar; GHSV, 6000 ml/g · h; pyridine concentration, 6500 ppm. The conversion was measured after a 10-h reaction.

[b] Pyridine HDN over the NiW carbide catalysts prepared using 20% CH_4/H_2 heated to 750°C.

[c] Pyridine HDN over the NiW carbide catalysts prepared using 10% C_2H_6/H_2 heated to 630°C.

The carbide catalysts were stable over 24 h, suggesting that under pressure conditions, the bimetallic carbide catalysts are stable, and Ni content has no significant effect on the catalyst stability. It is inferred from this that WC and $NiWC_x$ are the active components and are stable under the pressure conditions. The high H_2/CO ratio in the products over $Ni_{0.5}W_{0.5}C_x$ resulted from the decomposition of CH_4 over the catalyst; hence more carbon deposition is expected to occur over this catalyst. So a high Ni content is not suitable for the catalyst stability.

The results of the activity test of the $NiWC_x$ catalyst for hydrodenitrogenation are shown in Table 3. It is clear that the $NiWC_x$–*E* catalysts have higher pyridine conversion than does $NiWC_x$–*M*. The highest pyridine conversion over $NiWC_x$–*M* catalysts was 75.1%, which occurred for $Ni_{0.3}W_{0.7}C_x$–*M*. The catalyst containing 0.1 Ni had the lowest pyridine conversion, and this was only 45.7%. When the Ni content was 0.4 and 0.5 in $NiWC_x$–*M*, the pyridine conversions were 62.1 and 59.3%. This suggests that in the $NiWC_x$–*M* catalysts, Ni and W have a synergic effect on the HDN of pyridine, and the optimal composition for the bimetallic carbide catalyst prepared with CH_4/H_2 is $Ni_{0.3}W_{0.7}$. Over the $NiWC_x$–*E* catalyst, pyridine conversion is apparently higher than over $NiWC_x$–*M*, which may be due to a higher surface area and/or a different structure of the $NiWC_x$–*E*. As the Ni content changed from 0.1 to 0.4, the pyridine conversion increased from 62 to 88.6%, suggesting that the presence of more Ni in the $NiWC_x$–*E* improves the catalytic activity for pyridine HDN. However, the pyridine conversion over $Ni_{0.5}W_{0.5}C_x$–*E* dropped to 80.5%, suggesting that the optimal composition for $NiWC_x$–*E* for pyridine HDN is $Ni_{0.4}W_{0.6}$. This is different from the catalyst prepared using 20% CH_4/H_2.

CONCLUSION

The mixed-oxide $NiWO_4$ is formed by mixing and calcination of nickel nitrate and tungsten oxide. Addition of nickel nitrate up to the stoichiometric mixture does not lead to the formation of pure $NiWO_4$ under the preparation conditions.

Carburisation of $NiWO_x$ with methane produces WC carbide. The carburisation and the subsequent passivation lead to $NiWO_4$ on the carbide surface. The morphology of the $NiWC_x$ is different from both WC_x and Ni.

Carburisation of $NiWO_x$ with 10% C_2H_6/H_2 gives rise to W_2C carbides, and Ni is either in the lattice of W_2C or is highly dispersed on the carbide. Higher Ni content facilitates the carburisation of the oxide and leads to W_2C with larger particles than would otherwise be expected.

The $NiWC_x$ samples prepared with ethane have higher surface areas and smaller particle sizes than their methane congeners. The total carbon content in the $NiWC_x$ decreases with increasing nickel content.

The presence of Ni in the $NiWO_x$ decreases the carburisation temperature of WO_3 and helps the complete phase transformation from oxide to carbide.

The $NiWC_x$ catalysts prepared with 20% CH_4/H_2 and 10% C_2H_6/H_2 have almost the same activity and stability for partial oxidation of methane to synthesis gas. In pyridine HDN reaction, $NiWC_x$–*E* catalysts have higher activity than $NiWC_x$–*M* catalysts.

ACKNOWLEDGMENTS

T. Xiao thanks the Royal Society for a Royal Society BP-AMOCO fellowship. We thank CANMET and Colebrand for financial support for A. P. E. York, V. C. Williams.

REFERENCES

1. Chen, J. G., *Chem. Rev.* **96**, 1477 (1996).
2. Toth, L. E., "Transition Metal Carbides and Nitrides." Academic Press, New York, 1971.
3. Decker, S., Loefberg, A., Bastin, J. M., and Frennet, A., *Catal. Lett.* **44**, 229 (1997).
4. Volpe, L., and Boudart, M., *J. Solid State Chem.* **59**, 348 (1985).
5. Wrobleski, J. T., and Boudart, M., *Catal. Today* **15**, 349 (1992).
6. Chorley, R. W., and Lednor, P. W., *Adv. Mater.* **3**, 474 (1991).
7. Leclercq, L., Provost, M., Pastor, H., Grimblot, J., Hardy, A. M., Gengembre, L., and Leclercq, G., *J. Catal.* **117**, 371 (1989).
8. Giraudon, J.-M., Leclercq, L., Leclercq, G., Lofberg, A., and Frennet, A., *J. Mater. Sci.* **28**, 2449 (1993).
9. Zeng, D., and Hampden-Smith, M. J., *Chem. Mater.* **5**, 681 (1993).
10. Da Costa, P., Potvin, C., Manoli, J.-M., Breysse, M., and Djega-Mariadassou, G., *Catal. Lett.* **72**, 91 (2001).
11. York, A. P. E., Claridge, J. B., Williams, V. C., Brungs, A. J., Sloan, J., Hanif, A., Al-Megren, H., and Green, M. L. H., *Stud. Surf. Sci. Catal.* **130B**, 989 (2000).

12. Claridge, J. B., York, A. P. E., Brungs, A. J., and Green, M. L. H., *Chem. Mater.* **12**, 132 (2000).
13. Bouchy, C., Schmidt, I., Anderson, J. R., Jacobsen, C. J. H., Derouane, E. G., and Derouane-Abd Hamid, S. B., *J. Mol. Catal. A* **163**, 283 (2000).
14. Xiao, T. C., York, A. P. E., Williams, V. C., Al-Megren, H., Hanif, A., Zhou, X. Y., and Green, M. L. H., *Chem. Mater.* **12**, 3896 (2000).
15. Lofberg, A., Frennet, A., Leclercq, G., Leclercq, L., and Giraudon, J. M., *J. Catal.* **189**, 170 (2000).
16. Bouchy, C., Derouane-Abd, H., Sharifah, B., and Derouane, E. G., *Chem. Commun.* 125 (2000).
17. Schwartz, V., Oyama, S. T., and Chen, J. G., *J. Phys. Chem. B* **104**, 8800 (2000).
18. Oyama, S .T., Yu, C. C., and Ramanathan, S., *J. Catal.* **184**, 535 (1999).
19. Yu, C. C., Ramanathan, S., Dhandapani, B., Chen, J. G., and Oyama, S. T., *J. Phys. Chem. B* **101**, 512 (1997).
20. Xiao, T.-C., York, A. P. E., Al-Megren, H., Claridge, J. B., Wang, H.-T., and Green, M. L. H., *C. R. Acad. Sci.* **3**, 451 (2000).
21. Kim, C.-H., Yoon, W. L., Lee, I. C., and Woo, S. I., *Appl. Catal. A* **144**, 159 (1996).
22. Weitzel, H., *Z. Kristallogr. A* **144**, 238 (1976).
23. Chan, S. S., Wachs, I. S., and Murrell, L. L., *J. Catal.* **90**, 150 (1984).
24. Daturi, M., Busca, G., Borel, M. M., Leclaire, A., and Piaggio, P., *J. Phys. Chem. B* **101**, 4358 (1997).
25. Choudhary, T. V., and Goodman, D. W., *J. Catal.* **192**, 316 (2000).
26. Claridge, J., D. Phil. thesis. Oxford University, 1996.
27. Yvon, K., Nowotny, H., and Benesovsky, P., *Monatsh. Chem.* **99**, 726 (1968).
28. Palmer, D. J., and Dickens, P. G., *Acta Crystallogr. Sect. B* **35**, 2199 (1979).
29. Nagakura, S., *J. Phys. Soc. Jpn.* **13**, 1005 (1958).
30. Hanif, A., D.Phil. thesis. Oxford University, 2000.